ELSEVIER

Remote Sensing of Environment 77 (2001) 149–164

Remote Sensing of Environment

www.elsevier.com/locate/rse

Satellite observations of the microwave emissivity of a semi-arid land surface

June C. Morland[a], David I.F. Grimes[b,*], T.J. Hewison[c]

[a]*Meteorological Service of Canada Climate Research Centre, Downsview, Ottawa, Canada*
[b]*TAMSAT Group, Department of Meteorology, University of Reading, Earley Gate, PO Box 243, Reading RG6 6BB, UK*
[c]*UK Meteorological Office (Remote Sensing Division), Farnborough, UK*

Received 29 June 2000; received in revised form 30 January 2001; accepted 30 January 2001

Abstract

Microwave emissivity is an important parameter for rainfall estimation over land, as well as for atmospheric temperature and humidity retrievals. However, over land surfaces, it varies over a considerable range depending principally on vegetation cover and soil moisture. This study examines the feasibility of estimating emissivity from satellite-based vegetation and moisture indicators for a semiarid region in the African Sahel. Microwave emissivity was calculated from SSM/I observations at 19, 37, and 85 GHz horizontal (H) and vertical (V) polarisation. The technique was validated by comparing the measured emissivity of a sea surface area with the theoretically predicted emissivity. For a dry atmosphere, there was good agreement between theory and measurement. However, the discrepancy was considerably higher in an area where the atmosphere was humid, particularly at 85 GHz. This is attributable to increased uncertainty in atmospheric correction. The land surface emissivity over a 5° square area, which included the Hapex Sahel site, was studied from August to October 1992. The horizontally polarised emissivity e_H and polarisation difference measured over dry land areas were found to be well-correlated with Normalised Difference Vegetation Index (NDVI) such that NDVI can be used to estimate pixel e_H to within ± 0.02. For a wet land surface, there is a general trend for the emissivity to increase with increasing NDVI and for the polarisation difference to decrease. However, the trend is much less well defined than in the dry case. A weak relationship was observed between areal averages of previous day's rainfall (PDR) and emissivity for various vegetation cover classes. A similar relationship was observed with ground-based soil moisture measurements. The results show that emissivity can be estimated with a S.E. < 0.015 at 19 GHz from a combination of NDVI and rainfall or soil moisture information.

1. Introduction

Passive microwave satellite observations have an important role to play in meteorology and climatology. Knowledge of the microwave emissivity of the land surface is essential for the application of microwave data to temperature and humidity sounding (English, 1999), land surface temperature retrievals (Basist, Grody, Peterson, & Williams, 1998), and rainfall estimation over land (Xiang & Smith, 1997).

The research into microwave land surface emissivity described here has been motivated by a need to improve satellite-based rainfall estimates. In semiarid tropical areas such as the African Sahel, real-time rainfall measurements are vital for crop monitoring and drought and famine warning. Ground-based rain gauge networks are usually too sparse and do not provide timely information. On the other hand, satellite images are available in real-time and provide good spatial coverage. Most operational rainfall estimation systems for the tropics are based on thermal infrared (TIR) imagery from Geostationary satellites (e.g., Herman, Kumar, Arkin, & Kousky, 1997; Thorne, Coakeley, Grimes, & Dugdale, 2001). However, these techniques rely on indirect inference of rainfall from cloud top temperatures. Microwave imagery offers the potential for improvement because microwave radiation is strongly influenced by hydrometeors, and thus allows direct observation of rainfall and modelling of rainfall processes. Lower microwave frequencies (less than about 40 GHz) are most sensitive to the rain layer at the cloud base. Enhanced emission due to rain shows up well against the constant low emissivity background of the ocean allowing the retrieval of rainfall using model inversion techniques

* Corresponding author. Tel.: +44-118-9316693.
E-mail address: d.i.f.grimes@reading.ac.uk (D.I.F. Grimes).

0034-4257/01/$ – see front matter
PII: S0034-4257(01)00202-4

(Kummerow & Giglio, 1994). Over land, the background signal is both warmer and more variable than that from the ocean making reliable rainfall retrieval considerably more difficult. The variability of the land surface signal is due to variations in microwave emissivity caused by moisture, vegetation, and surface roughness. A major step forward would be the ability to estimate microwave emissivity from remote observations of vegetation and soil moisture. This paper examines the feasibility of making such estimates using satellite data. It follows on from work done using airborne radiometers reported in Morland, Grimes, Dugdale, and Hewison (2000).

The emissivity of a surface at a given wavelength is defined as the ratio of the actual emission of electromagnetic radiation from a surface at that wavelength to the emission, which would be expected from a blackbody at the same temperature.

The relationship between temperature and radiance is approximately linear at microwave wavelengths (the Rayleigh Jeans approximation; Ulaby, Moore, & Fung, 1981). Ignoring atmospheric effects between the surface and the radiometer, T_o, the brightness temperature of the upwelling surface radiation can be written in terms of T_p, the physical temperature of the surface, T_a, the brightness temperature of the downwelling atmospheric radiation, and e the surface emissivity.

$$T_o = eT_p + (1 - e)T_a$$

from which

$$e = \frac{T_o - T_a}{T_p - T_a} \quad (1)$$

where all variables apart from T_p are a function of frequency ν.

To retrieve surface emissivity from the satellite data, T_a and T_p must be estimated and T_o as observed by the satellite must be corrected for the effects of the intervening atmosphere. The details of how these corrections were carried out in this study are given in Section 4.

2. Emissivity measurements

2.1. Measurements using ground and aircraft observations

In the frequency range of interest to passive microwave rainfall algorithms (about 20–90 GHz), ground or aircraft-based measurements of surface emissivity have been made by a number of workers (e.g., Calvet, Wigneron, Chanzy, & Haboudane, 1995; Mätzler, 1994; Morland et al., 2000; Wigneron, Kerr, Chanzy, & Jin, 1993). The results indicate that soil emissivity decreases with increasing water content and the magnitude of the change is smaller at higher frequencies. The effect of vegetation is relatively small at low frequencies, but above 15 GHz, it may mask changes in soil moisture emission. For example, Jackson (1997) shows that 20-GHz emissivities have almost no sensitivity to soil moisture in the presence of vegetation with a water content of 1 kg m^{-2}. Thus, soil moisture and vegetation cover are important parameters in determining surface emissivity viewed from the satellite. Soil roughness also has an important role to play in that it increases soil emissivity, and hence counteracts the effect of increases in soil moisture (Choudhury, Schmugge, Chang, & Newton, 1979). Other factors, which have a minor or negligible effect on emissivity at these frequencies, are soil texture, rock fraction, organic matter content, temperature, and salinity (Hallikainen, Ulaby, Dobson, El-Rayes, & Wu, 1985; Jackson, Kostov, & Saatchi, 1992; Jackson & O'Neill, 1988; Sreenivas, Venkataratnam, & Narasimha Rao, 1995).

The three main influences on microwave emissivity — soil moisture, vegetation cover, and soil roughness — all vary temporally. This means that the emissivity at a given location is continually changing and cannot be defined by a single measurement. However, it may be possible to relate the emissivity to the factors influencing it, and thus produce a means of predicting microwave emissivity from other data. In a previous publication (Morland et al., 2000), we have explored the feasibility of this approach using aircraft mounted sensors. In this paper, we extend the study to satellite observations.

2.2. Measurements using satellite data

Choudhury (1993) calculated monthly averages of 19 and 37 GHz horizontally (H) and vertically (V) polarised reflectivity (where reflectivity = 1 − emissivity) for 1988 and 1989 over two desert and two vegetated sites in Africa. He gridded SSM/I data into $0.25° \times 0.25°$ cells and studied a 9×9 cell area around each site of interest. The difference between the H and V brightness temperatures was calculated, and the data with the second lowest polarisation difference were kept for each 10-day period with the aim of minimising the effect of clouds and soil moisture variations. The brightness temperatures for each 10-day period were then averaged to give a monthly mean. Ground meteorological data were used to obtain surface temperature and atmospheric corrections. Available meteorological data were coincident with the rainforest and savannah locations, but not with the desert location. Choudhury took daily mean air temperature, adjusted for the time of the SSM/I overpass, to be the ground temperature. Monthly mean surface vapour pressure and daily mean surface temperature were used to calculate downwelling microwave radiation and correct upwelling microwave radiation for atmospheric effects.

This is a very simple method of calculating reflectivity and emissivity, using only SSM/I observations and meteorological measurements averaged over daily or monthly periods. One major problem is that the air temperature measured at 2 m is often dissimilar to the ground temperature, especially over bare soil surfaces. However, the

method was sensitive enough to show a seasonal variation in the reflectivity measured at the savannah site. The reflectivity difference varied from 1% at a time of full vegetation growth to 4% in the dry season. This suggests that the monthly averaging of the results compensate for the simplicity of the approach.

Prigent, Rossow, and Matthews (1997) also made monthly estimates of emissivity. However, their method was more sophisticated in that surface temperature was derived from daily infrared satellite observations. They also used daily remotely sensed temperature and water vapour soundings to calculate atmospheric corrections. They calculated emissivity for the Meteosat viewing area (Africa, Western Asia, and Europe) for all SSM/I channels (19 GHz H and V, 22 GHz V, 37 GHz H and V, 85 GHz H and V). The grid spacing of the emissivity estimates was 25–30 km. The study covered March, July, October, and December 1991.

Infrared data from the International Satellite Cloud Climatology Project (ISCCP) at a spatial resolution of 30 km and temporal resolution of 3 h were used to identify clouds. Prigent et al. (1997) used a threshold of 260 K to eliminate cloudy data. They reasoned that thin cirrus could be tolerated because it would have a negligible effect on SSM/I observations. Atmospheric water vapour and temperature data were obtained from daily satellite soundings. These were available at a spacing of approximately 2.5° in latitude and longitude. The atmospheric soundings were used to calculate surface temperature from the ISCCP data assuming a TIR emissivity of 1.0. Because the infrared dataset had a temporal resolution of only 3 h, the data were interpolated to the time of the SSM/I pass. They did not specify how this affected cloud masking since clouds can evolve considerably within a 3-h period. The remotely sensed atmospheric water vapour and temperature profiles were used to calculate downwelling microwave radiation and to correct for the effect of the atmosphere on upwelling microwave radiation.

Jones and Vonder Haar (1997) used a similar method to Prigent et al., but calculated daily emissivity at SSM/I frequencies across the USA for 70 days in summer to autumn 1991. Surface temperature was derived from TIR data obtained within 10 min of the SSM/I overpass. Infrared and microwave atmospheric corrections were carried out using temperature and water vapour profiles from an upper air dataset. Interpolation was carried out between profiles where necessary. The surface pressure was adjusted for ground elevation using digital elevation model data. Cloud contaminated areas were identified by low or negative infrared atmospheric corrections. Some low fog escaped detection, lowering the surface temperature by about 2 K, but this was thought to have a negligible effect on the emissivity results. Jones and Vonder Haar show that neglecting atmospheric effects in the surface emissivity calculation can cause errors of up to 40% at 85 GHz if the surface emissivity is low. They present their emissivity results in the form of composited imagery. Unfortunately, the computed emissivities are not verified against independent data, rather the images are discussed in terms of their ability to identify surface features.

Xiang and Smith (1997) took quite a different approach to emissivity calculation. By combining data from two overpasses, they were able to solve a set of radiative transfer equations for surface temperature and emissivities at 19, 37, and 85 GHz. This method is restricted to cloud free areas for which two SSM/I passes overlap on the same day. The method also assumes that emissivity does not change during the day, which would not necessarily be the case if there was a significant change in soil moisture between the two observation times. The retrieval algorithm produced an average, unpolarised emissivity value at each frequency. Xiang and Smith applied the method to the area surrounding the Hapex Sahel study field site for a few days in 1992.

The emissivities were used as boundary conditions for a physically based precipitation retrieval algorithm. Rain rates calculated from the SSM/I measurements showed some agreement with rain rates calculated from the EPSAT rain gauge network. These results suggest that land surface emissivity information can indeed improve microwave rainfall estimation techniques over land.

3. The study area

The area selected for this study was the Hapex Sahel experimental site and surrounding area (0°–5°E and 11°–16°N). Emissivity was calculated for a 92-day period from 1st August to 31st October 1992. This covered the transition from the wet to the dry season, allowing the emissivity to be estimated for different soil moisture conditions. The Hapex Sahel area was chosen because it was the site of an intensive measurement campaign in 1992 and many ground measurements were available. The EPSAT rain gauge network is located in this area (see Lebel, Sauvageot, Hoepffner, Desbois, Guillot, & Hubert, 1992). It extends from 1.6° to 3.3°E and 13.0° to 14.0°N and provides rainfall observations at a resolution of about 12.5 km. There was an increased rain gauge density over sites of special interest (known as super sites). The study area is also interesting because of the change in vegetation cover from dense vegetation in the extreme south, classified in Matthews (1983) as tropical drought-deciduous forest, and very little or no vegetation in the north, classified in Matthews (1983) as desert.

4. Method of emissivity measurement

4.1. General approach

Emissivity was estimated from the satellite data via Eq. (1). For this calculation, measurements are required of T_o, T_a, and T_p. Additionally, atmospheric temperature and

humidity information is required to correct for atmospheric effects between the radiometer and the surface.

The observed microwave brightness temperature, T_o, was obtained from SSM/I imagery, the effective atmospheric brightness temperature, T_a, was calculated from the European Centre for Medium Range Weather Forecasting (ECMWF) model analyses of atmospheric temperature and humidity profiles. The use of radiosonde data was also considered, but trials showed that they contained many errors and instabilities, and therefore the model data into which some radiosonde data has been assimilated was preferred. The physical surface temperature, T_p, was estimated from Meteosat TIR imagery at the time closest to the SSM/I overpass. Both T_o and T_p were corrected for atmospheric effects using the method described below. Emissivities were calculated for all SSM/I frequencies.

4.2. Data preparation

The SSM/I instrument is carried on board the US DMSP polar orbiting satellite and has seven channels. These correspond to H and V polarisations at 19.35, 37.0, and 85.5 GHz and a V only polarisation at 22.235 GHz. A point on the Earth's surface in the tropics is sampled with a frequency of at best once to twice daily. Table 1 gives the 3-dB field of view of the SSM/I channels.

SSM/I brightness temperatures were extracted for the area of study and projected onto a 5° square latitude/longitude grid. The SSM/I data were oversampled in the reprojection to achieve a similar resolution to Meteosat TIR imagery ($\sim$5 km). Each reprojected image was 128×128 pixels, giving a resolution of 0.039° per pixel. This is also conveniently a multiple of the resolution of the AVHRR dataset (512×512 pixels) used in estimating vegetation cover.

Cloudy areas in the SSM/I images were identified using Meteosat TIR imagery. Meteosat images are transmitted every 30 min, so this meant that a TIR image was usually available within 15 min of an SSM/I overpass. When a TIR image was missing, the time gap could be as great as half an hour. The Meteosat raw data were converted to temperature in Kelvin and projected onto the same grid as the SSM/I data.

Although passive microwave data is relatively unaffected by thin, nonraining cloud, this is not true for the TIR data, which provided the surface temperature information. A cloud mask was therefore applied to the TIR images. An examination of near surface air temperature, measured by Monteny (1995) in the Hapex Sahel study area, showed that air temperature was never lower than 290 K at the time of the morning pass and 295 K at the time of the afternoon pass. These values were adopted as the threshold for the cloud mask.

There was occasionally some discrepancy between the TIR cloud mask and the microwave data affected by cloud. This was not surprising given that the two images could be up to half an hour apart. In addition, even if there is no temporal discrepancy, the microwave pixels are much larger than the infrared pixels and can be affected by partial cloud filling. To avoid this, pixels were rejected if the 85-GHz V emissivity was lower than 0.85 on the basis that cloud top ice causes scattering in this channel and reduces the retrieved emissivity. The final cloud masking criteria were stringent to ensure data quality. This meant that some wet days were not included in the analysis because they contained insufficient clear data.

Table 1
The 3-dB field of view of the SSM/I channels

Frequency (GHz)	Field of view (km)
85.5 H and V	16×14
37.0 H and V	38×30
22.235 V	60×40
19.35 H and V	70×45

4.3. Upwelling microwave temperature, T_o

The observed upwelling microwave temperature as seen by a satellite at height h must be corrected for the effects of the intervening atmosphere to give the temperature, which would be observed at ground level for insertion in Eq. (1). This correction was carried out using a microwave radiative transfer program developed at the UK Meteorological Office (English, 1995). The ECMWF analyses of temperature and water vapour at 14 levels (European Centre for Medium Range Weather Forecasting, 1995) were used to provide temperature and humidity profiles for the model inversion. The profiles were on a latitude/longitude grid at a spacing of 0.5° giving 121 profiles in all. The analysis data are available on a 6-h time step and the closest in time to the SSM/I overpass (either 6 a.m. or 6 p.m.) was used. The atmospheric contribution for each pixel on the image was calculated from the nearest ECMWF profile grid point.

4.4. Downwelling microwave temperature, T_a

The same radiative transfer program and ECMWF analysis data as described above were used to calculate the downwelling atmospheric brightness temperature measured at the surface T_a for each pixel.

4.5. Surface temperature, T_p

The closest Meteosat TIR image to each SSM/I overpass was used to calculate surface temperature (T_p). The Rayleigh Jeans approximation is less accurate at infrared wavelengths, and therefore the calculation was carried out in terms of radiance.

The radiance L_o observed at the top of the atmosphere (height, h) can be expressed as

$$L_o(h) = \tau e_{IR} B(T_p) + \tau(1 - e_{IR}) L_{a\downarrow}(0) + L_{a\uparrow}(h) \qquad (2)$$

where B is the Planck function integrated over the radiometer response function, τ is the atmospheric transmissivity, e_{IR} is the infrared emissivity of the surface, $L_{a\downarrow}(0)$ is the downwelling radiance at the surface (height = 0), and $L_{a\uparrow}(h)$ is the upwelling radiance from the atmosphere at height h. Eq. (2) can be conveniently rewritten as

$$L_o(h) = e_{IR}B(T_p) + (1 - e_{IR})L_{a\downarrow}(0) + L_{corr} \quad (3)$$

where the first two terms on the right-hand side represent the upwelling radiance, which would be observed at ground level, and L_{corr} is a correction for absorption and emission by the atmosphere of the total upwelling radiance.

Rearranging Eq. (3) gives

$$B(T_p) = \frac{L_o(h) - (1 - e_{IR})L_{a\downarrow}(0) - L_{corr}}{e_{IR}} \quad (4)$$

from which T_p can be obtained by inverting the Planck function. Thus, to calculate T_p, we need values for $L_o(h)$, e_{IR}, $L_{a\downarrow}(0)$, and L_{corr}.

$L_o(h)$ is obtained directly from the Meteosat data.

The downwelling radiance at ground level $L_{a\downarrow}(0)$ was calculated from $L_o(h)$ using an infrared radiative transfer program (Shine, 1991). The program was adapted to take account of the Meteosat TIR radiometer response function (Meteosat Exploitation Project, 1989). The same 121 ECMWF analysis profiles used in the calculation of the microwave atmospheric correction were used as input to the radiative transfer calculation.

To calculate L_{corr}, it was observed that there was a linear relation between L_{corr} calculated from the model and the modelled upwelling radiance at the top of the atmosphere $L_{om}(h)$. Fig. 1 shows an example for three locations on 2nd August 1992. Values are plotted for T_p between 270 and 310 K. For each day and each of the 121 ECMWF grid points in the $5° \times 5°$ target area, L_{corr} and $L_{om}(h)$ were calculated from the ECMWF profiles and parameters for the linear relationship were obtained. These parameters were then used to calculate L_{corr} from the observed $L_o(h)$ for all pixels in the 128×128 grid.

The infrared emissivity e_{IR} was calculated from 10-day Normalised Difference Vegetation Index (NDVI) maximum value composites. Van de Griend and Owe (1993) used experimental ground data obtained in Botswana to show that there was a nonlinear relationship between NDVI and TIR emissivity. Valor and Caselles (1996) provided a theoretical basis for this relationship and showed how it could be applied to satellite data. The method requires knowledge of local values of the TIR emissivity for bare soil and full vegetation cover. It also requires some assumptions about the dimensions and spacings of the vegetation. Valor and Caselles give an example of the implementation of the method over the Hapex Sahel area and provide coefficients for this region. Their methodology and coefficients were used here.

Using the results described above, $B(T_p)$ and hence T_p were calculated at each grid point via Eq. (4). The Meteosat response function was taken into account when inverting the Planck function.

4.6. Check on surface temperature calculation

The surface temperature calculation was checked by comparing air temperature and soil temperature measured at ground level during Hapex Sahel with the satellite temperature for the same location. The problem here is that point measurements are being compared with 5×5 km pixel average temperatures. However, it should give some indication of the effectiveness of the surface temperature calculation.

Measurements of air temperature at 1.4 m were recorded by Monteny (1995) at 2.7°E, 13.5°N (referred to from now on as site M) and by Dugdale (1995) at 2.2° E, 13.2° N (referred to from now on as site D). Soil temperatures at 2-cm depth were also available for site M. These were compared

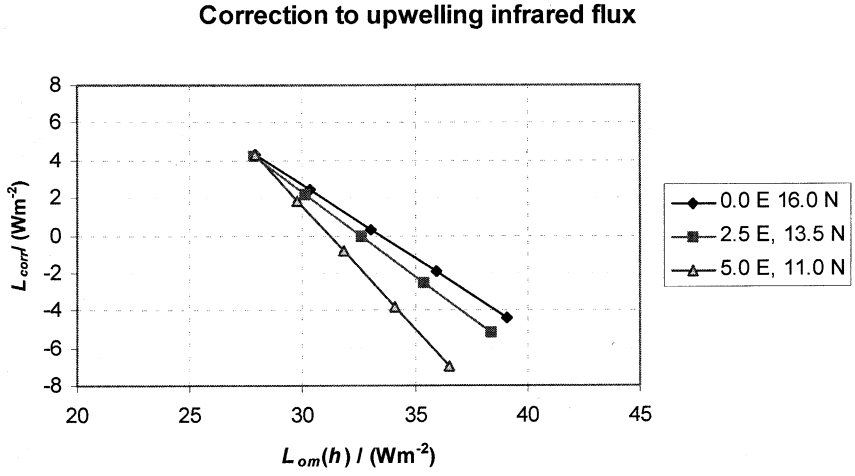

Fig. 1. The relationship between modelled upwelling TIR radiance at the top of the atmosphere $L_{om}(h)$ and the correction to convert to upwelling radiance at the surface L_{corr} at three locations in the HAPEX Sahel area on 02/08/92. Input surface temperatures ranged from 270 to 310 K.

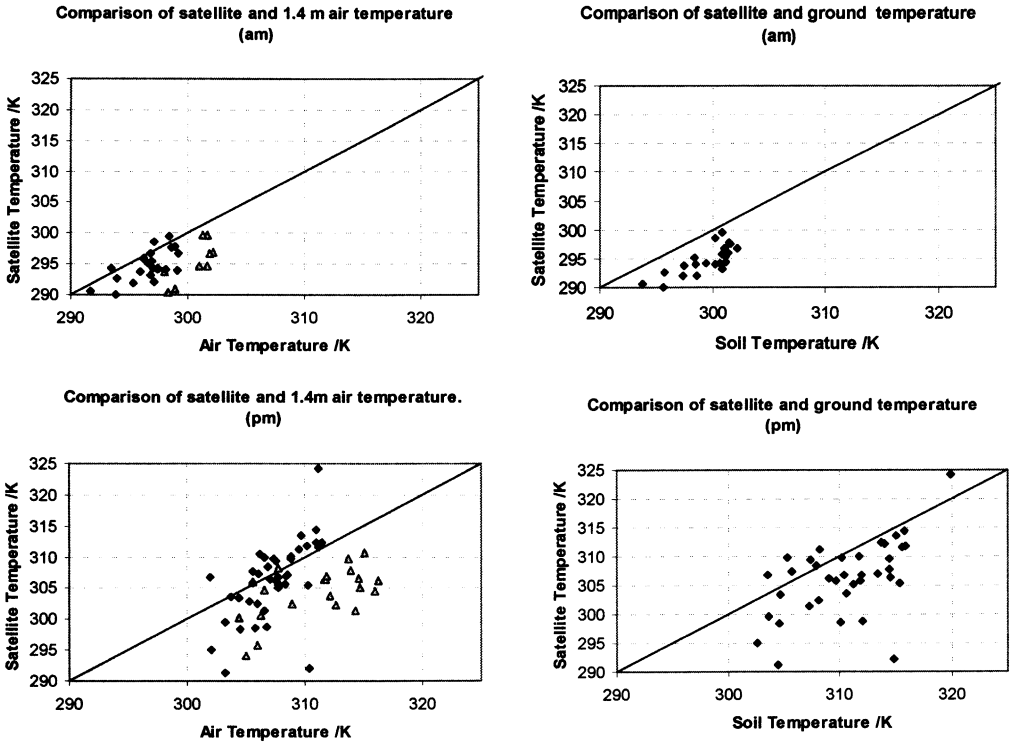

Fig. 2. Soil temperature (2 cm depth) and air temperature observations compared with surface temperature calculated from Meteosat TIR imagery for the corresponding 5 × 5 km pixel for times coincident with the SSM/I overpasses (morning and afternoon). The open triangles represent site D and the filled diamonds represent site M.

with satellite T_p values for the corresponding pixel. Fig. 2 shows the ground and satellite data compared for times coincident with the SSM/I morning and afternoon passes. All cases where the satellite temperature was not affected by cloud (i.e., $T > 290$ K) were included in the comparison. The mean difference and root mean square difference (RMSD) between satellite TIR temperatures and ground-based measurements are summarised in Table 2. Fig. 2 shows a rough correspondence between the ground-based observations and the satellite estimates. Interestingly, the closest agreement is with the afternoon air temperatures at site M.

Consideration of Table 2 suggests that the satellite is systematically underestimating the surface temperature by a few degrees. This may be due to inadequacies in the atmospheric correction. However, it is difficult to be certain because comparison is being made between point measurements and pixel averages. It may be that the two sites used are not representative of the respective pixels. Albedo, vegetation, wind speed and direction, surface moisture, and shading may all affect local conditions and as these are not known more quantitative conclusions about the satellite error cannot be drawn.

4.7. Microwave emissivity calculation

Microwave emissivities in all SSM/I channels at both H and V polarisations were calculated via Eq. (1) after correction for atmospheric emission and absorption as described above. Fig. 3a shows an example of the 85-GHz H emissivity for the 5° square on the 26th of October 1992 when the atmosphere was clear and the surface dry. It may be compared to the NDVI composite image for the last decade in October in Fig. 3b. It can be seen that there is a rough correspondence between the spatial patterns of NDVI and emissivity. Both parameters show a general increase from north to south, and in both images the Niger River is visible running diagonally across the images from NW to SE.

It is not easy to calculate an error on the final emissivity estimate because errors in the data used are difficult to evaluate. Validation of the estimated emissivities will be dealt with in Section 4.8. Possible sources of error are:

- Satellite instrument errors,
- Errors in ECMWF water vapour and temperature profiles

Table 2
Mean differences (MD) and RMSD between satellite TIR temperatures (T_{sat}) and ground-based measurements (T_{obs}) for air temperatures measured at 1.4 m and soil temperatures at 2 cm depth

	Site M		Site D	
	MD (K)	RMSD (K)	MD (K)	RMSD (K)
Air	−1.9	2.7	−5.4	5.8
	−4.8	5.1		
	−1.0	4.9	−6.4	7.4
	−4.2	7.0		

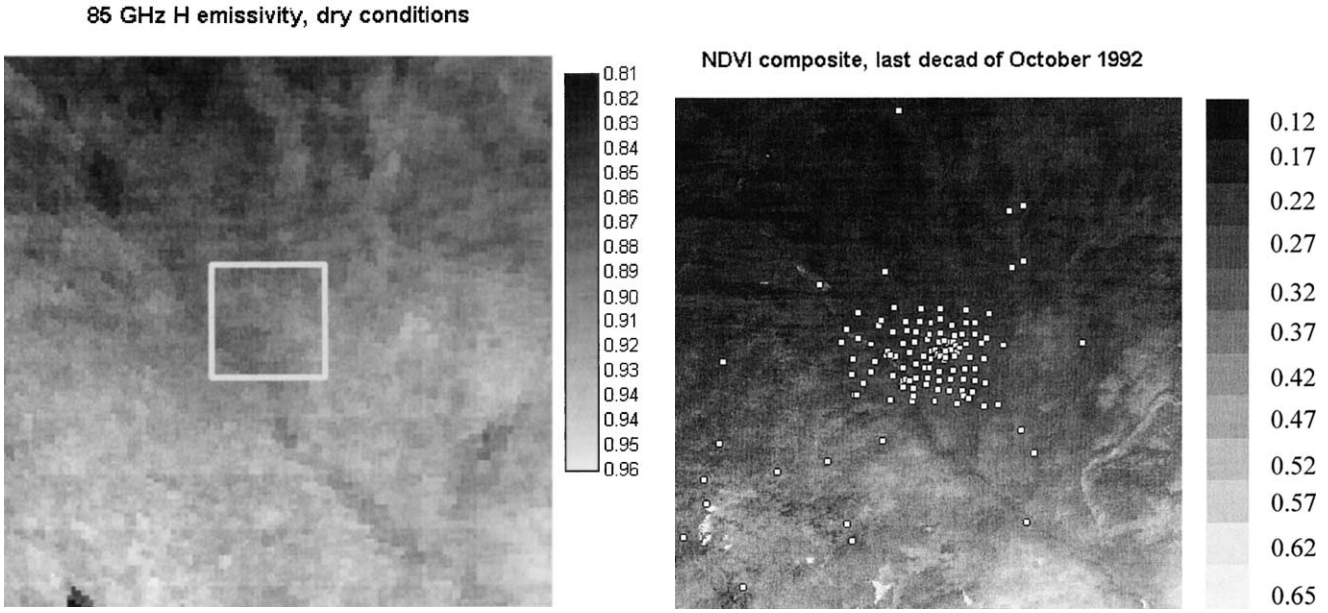

Fig. 3. (a) 85 GHz H emissivity measured for the area 0° to 5° E and 11° to 16° N on 26/10/92. The white line indicates the 1 degree square shown in Fig. 4. (b) NDVI calculated for the same area as Fig. 3a over the last dekad of October 1992. Each white circles represents a raingauge.

- Errors in model calculation of atmospheric correction for infrared and microwave data
- Inadequate cloud masking due to time lag between microwave and infrared observation or due to microwave pixels being partially filled by cloud.

4.8. Check on microwave emissivity calculation

The accuracy of the emissivity estimates for open water can be assessed by comparing them with theoretical model values.

Two water targets were used for this evaluation:

- A sea, coast, and land area where the atmosphere would normally be very dry (14.0°–19.0°W and 19.0°–24.0°N).
- A sea, coast, and land area where the atmosphere would normally be humid (0.5°–5.5°E and 4.0°–9.0°N).

A mainly cloud free sea area with dry atmosphere was extracted for the afternoon pass on 25th October 1992. Two mainly cloud free areas with moist atmosphere were extracted from the morning passes on 25th and 26th October 1992. The emissivity was calculated at each of the SSM/I frequencies using the microwave data, coincident METEOSAT TIR imagery, and ECMWF profiles of temperature and water vapour at 0.5° spacing.

The emissivities were calculated theoretically using the model described by English and Hewison (1998). This takes into account the effects of frequency, temperature, salinity, wind, surface swell, small-scale roughness, and the presence of foam. The model requires information on frequency, temperature, view angle, wind speed, and salinity.

Horizontal wind speed at 10-m height and 0.5° spacing was extracted from the ECMWF daily analysis for the areas of interest. Salinity was fixed at 35‰ for the sea surface. In each case, the average TIR temperature of the water body after land had been masked off was used as the input surface temperature. The wind speed was allowed to vary across the grid squares when calculating the emissivity. Input parameters are summarised in Table 3.

Table 4 shows the mean theoretical and observed sea surface emissivity for the three examples. It shows that there is a good agreement between the average emissivities calculated and observed over the sea surface where the atmosphere is dry. The agreement is to within 0.01 at 19 GHz, 0.015 at 22 and 37 GHz, and 0.035 at 85 GHz. As might be expected, there is weaker agreement for the area with the moist atmosphere, which indicates that errors in the atmospheric profiles or atmospheric correction are contributing to errors in the emissivity. The greatest discrepancies (up to 0.17) are for the 85-GHz H polarisation. At this frequency, there is greater sensitivity to changes in the atmospheric profile. Errors at other frequencies are ≤ 0.07 on 25th October 1992 and < 0.05 on 26th October 1992

Table 3
Input parameters for calculation of sea surface emissivity

Date	25 October 1992	26 October 1992
View angle (°)	53	53
Salinity (‰)	35	35
Surface temperature (K)	296.5	298.9
Mean windspeed (m s^{-1})	2.3	1.6

Table 4
Comparison of mean theoretical and observed emissivity over the sea surface for areas with dry and moist atmospheric profiles

		Emissivity			Theoretical – observed emissivity	
Date and time	Frequency (GHz)	Theoretical	Observed (atmospheric correction)	Observed (no atmospheric correction)	Atmospheric correction	No atmospheric correction
25 October 1992, 1601, dry atmosphere	19.35 H	0.274	0.281	0.389	−0.007	−0.115
	19.35 V	0.575	0.581	0.643	−0.006	−0.068
	22.235 V	0.586	0.572	0.702	+0.014	−0.116
	37.0 H	0.325	0.331	0.468	−0.006	−0.143
	37.0 V	0.644	0.629	0.703	+0.015	−0.059
	85.5 H	0.417	0.392	0.664	+0.025	−0.247
	85.5 V	0.756	0.722	0.842	+0.034	−0.086
25 October 1992, 0516, moist atmosphere	19.35 H	0.273	0.339	0.542	−0.066	−0.269
	19.35 V	0.570	0.615	0.730	−0.045	−0.160
	22.235 V	0.579	0.646	0.854	−0.067	−0.275
	37.0 H	0.318	0.373	0.586	−0.055	−0.268
	37.0 V	0.628	0.652	0.766	−0.024	−0.138
	85.5 H	0.404	0.578	0.880	−0.174	−0.476
	85.5 V	0.736	0.807	0.932	−0.072	−0.196
26 October 1992, 0445, moist atmosphere	19.35 H	0.273	0.315	0.511	−0.042	−0.238
	19.35 V	0.571	0.602	0.713	−0.031	−0.142
	22.235 V	0.580	0.618	0.829	−0.037	−0.249
	37.0 H	0.316	0.346	0.557	−0.030	−0.241
	37.0 V	0.629	0.638	0.750	−0.008	−0.121
	85.5 H	0.403	0.518	0.852	−0.116	−0.449
	85.5 V	0.737	0.781	0.919	−0.043	−0.182

Jones and Vonder Haar (1997) analysed the error that occurs in the emissivity calculation if the atmosphere is ignored. They found that the error due to atmospheric effects increases as the surface emissivity decreases. This is because of the greater contribution to the observed radiance made by atmospheric upwelling and reflected downwelling radiation. They also observed that the 85-GHz channel is more affected by water vapour than the lower frequencies, which is consistent with the observations in Table 4. Similar results are reported by Prigent et al. (1997).

For land surfaces, we would expect emissivities ranging between 0.7 and 0.95, and therefore the errors due to atmospheric correction should be lower than for the sea surface. Table 4 gives only one sample for a dry atmosphere and two for moist conditions; nevertheless, we can use it as a conservative indicator that at frequencies <40 GHz we should expect emissivity errors <0.015 over land in a dry atmosphere and <0.07 in a moist atmosphere. At 85.5 GHz, the corresponding numbers are <0.035 (dry) and 0.17 (moist).

5. Vegetation cover and soil moisture information

The main aim of this project is to investigate the dependence of land surface microwave emissivity on vegetation and soil moisture with a view to improving rainfall estimation. The complete spatial coverage of vegetation and soil moisture required for comparison with the emissivity retrievals is only feasible using satellite imagery. In this work, we have used the NDVI to estimate vegetation cover. Unfortunately, no remotely sensed soil moisture measurements are available from a satellite platform at present, therefore, we have tried three alternative indicators. These are:

(i) Previous day's rainfall (PDR)
(ii) Ground-based soil moisture measurements from the Hapex Sahel experiment
(iii) Antecedent Precipitation Index (API)

5.1. Calculation of NDVI

The NDVI is based on the fact that vegetation and soil have similar reflectivities in the red region of the spectrum, but vegetation has a higher near-infrared reflectivity than soil. The NDVI is defined as follows, where ρ_R and ρ_{NIR} are red and near-infrared reflectivity, respectively (Eq. (5)).

$$\mathrm{NDVI} = \frac{\rho_{NIR} - \rho_P}{\rho_{NIR} + \rho_R} \tag{5}$$

In this case, ρ_R and ρ_{NIR} were obtained from Channels 1 (0.58–0.68 μm) and 2 (0.725–1.1 μm) observations made by

the AVHRR polar-orbiting satellite. The reflectivity data for the Hapex Sahel area (0°–5°E and 11°–16°N) were obtained from the Hapex Sahel database. The processing of AVHRR observations to produce reflectivities was carried out by Kerr, Lagouarde, and Imbernon (1992). A cloud mask was applied to this data set before the NDVI was calculated. Cloud was identified as having a combination of low temperature and high reflectivity relative to the land surface. All AVHRR Channel 5 brightness temperatures (11.5–12.5 μm) less than or equal to 283 K were reclassified as 283.1 K. A cloud index was then calculated as $\rho_R/(T_{5*} - 283)$ where T_{5*} denotes the reclassified temperatures. High values of this index indicate cloud. A number of cloud index images from different months and times of day were examined to determine the optimum cloud threshold. The delineation between cloud and land was not always clear cut but a threshold was assigned, which varied according to the time of day but did not change from month to month.

Any cloudy pixels distinguished by the cloud index threshold were set to zero. The NDVI was calculated over approximately 10-day periods according to data availability. A maximum value composite was created by taking the maximum observed NDVI for each pixel. Since cloud or water vapour lowers the observed reflectivity values, the highest NDVI value for each pixel in a 10-day series is the observation least affected by cloud and water vapour. Fig. 3b shows a sample NDVI image.

The composites covering August and September had some zero values where there was persistent cloud over the area, as well as pockets where the NDVI was considerably lower than in surrounding areas due to water vapour absorption. Calculation of the local interpixel NDVI gradient allowed areas where the NDVI decreased suddenly to be identified and masked.

5.2. Soil moisture information

5.2.1. Previous day's rainfall

The simplest indirect indicator of soil moisture is the PDR (measured at 6 a.m. and assigned to the preceding day). Most rainfall in the region occurs between afternoon and nighttime. As little evaporation takes place at night but rapid evaporation occurs during daylight hours, it might be expected that this method would give a reasonable representation of near surface moisture for morning SSM/I overpasses.

Fig. 3b shows the rain gauges available for the study against the background of an NDVI image. The high concentration observable in the centre of the image is the EPSAT dense network with gauges spaced at approximately 12-km intervals. In contrast, there are very few rain gauges outside this area. Some 1° squares contain no rain gauges whatsoever. The geostatistical technique of block kriging (Journel & Huijbregts, 1978) was used to generate a rainfall field with the same spatial resolution as the satellite data. In order to increase the amount of data available for the kriging process, all rain gauges between 1°W and 6°E and 10°–17°N were included. This gave a total of 176 rain gauges of which 100 lay in the Hapex Sahel 1° square.

5.2.2. Ground-based soil moisture measurements

Some direct soil moisture measurements were available for a number of sites in the study area (Fig. 4) as part of the Hapex Sahel experiment. Different techniques were used at different sites including gravimetric analysis, time domain reflectometry, and neutron probe measurements. The data were obtained from the Hapex Sahel CD-ROM (Chanzy, 1995; Cooper, 1995; Stricker, 1995). Measurements were made at a range of depths down to 2 m. As microwave emission at SSM/I frequencies is mainly determined by the topmost layers of soil, only estimates from depths above 10 cm are considered here. Within this depth range, measurements were available for 0–0.5, 0.5–2, 0–5, and 0–10 cm. However, sufficient days of coincident soil moisture and emissivity estimates were present only for the 0–5-cm range. Therefore, the analysis in subsequent sections focuses on this depth. Six of the sites in Fig. 4 recorded 0–5 cm soil moisture. Measurement times varied but were usually morning or early afternoon.

5.2.3. Antecedent Precipitation Index

A third approach to soil moisture estimation is the calculation of an API. This is a simple indicator of moisture in the upper soil layers and is described in detail by Choudhury and Blanchard (1983). The API on a specific day is calculated from rainfall and potential evaporation history, as well as information on soil characteristics. In this study, daily API was calculated from kriged rain gauge observations and potential evaporation data obtained from

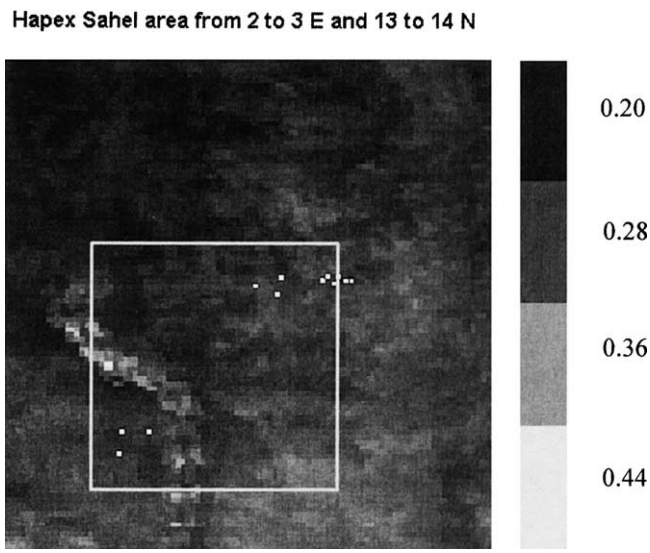

Fig. 4. Soil moisture sites available from HAPEX-Sahel shown as white squares against the background of an NDVI image for the area 2° to 3° E, 13 °to 14° N. The white line indicates the 0.5° square over which emissivity estimates were averaged for comparison with soil moisture measurements.

the Hapex Sahel study (Monteny, 1995). It was found that the API was in every case less well correlated with emissivity than was the PDR. This may be because, in semiarid areas, near surface moisture dries out within a few hours of a rainfall event, and the API places too much emphasis on past rainfall. In the following sections, only results using PDR and soil moisture measurements are reported.

6. Relationship between emissivity and vegetation cover

6.1. Dry conditions

For the month of October, when the area was mainly dry, the emissivity data were compared with the appropriate 10-day NDVI composite.

Fig. 5 shows the H polarisation emissivity e_H and V–H polarisation difference($e_V - e_H$), at 19, 37, and 85 GHz for each pixel plotted against NDVI for 26th October 1992, a dry day. The SSM/I data were acquired during the morning pass. The whole of the 5° square was cloud free, and no rain had fallen since the 24th October 1992 when four stations had reported rainfall.

It can be seen that the e_H increases nonlinearly and ($e_V - e_H$) decreases nonlinearly with NDVI. The V polarisation emissivity, e_V, was relatively independent of the vegetation index. The maximum ($e_V - e_H$) is 0.15, 0.12, and 0.10 at 19, 37, and 85 GHz, respectively. The minimum e_H is 0.84, 0.83, and 0.83 at 19, 37, and 85 GHz, respectively.

In order to define a representative curve for dry conditions, eight passes were selected for which the study area was almost certainly dry. From the 21st to the 31st October, the only rain recorded was at four gauges on the 24th. The images used in the dry study were the morning passes on 23rd, 24th (rain had not yet fallen), 26th, 27th, and 31st October and the afternoon passes on 25th, 30th, and 31st.

An empirical function of the form (Eq. (6))

$$e = a + b\log_e(Nc) \tag{6}$$

was fitted to the data. Here, e represents either e_H or $e_V - e_H$, N is the NDVI, and a, b, and c are empirical coefficients to be optimised.

The mean a, b, and c coefficients, the mean correlation coefficient, r^2, and the standard deviation of the coefficients were calculated and listed in Table 5.

Table 5 shows that there is little variation with frequency in the fit between e_H and NDVI. The mean value of r^2 increases slightly with decreasing frequency and is higher for ($e_V - e_H$) than for e_H. The standard deviation of the a and c coefficients is about 1% of their value, and the standard deviation of the b coefficient is about 10% of its value. Varying the a, b, and c coefficients by 1 S.D. causes emissivity changes of ±0.012, ±0.008, and ±0.001, respectively.

The emissivity for the morning pass on 26th October 1992 was calculated from the 10-day NDVI composite using the mean dry curve coefficients given in Table 5. The last column of the table gives the mean absolute difference (MAD) between the measured and calculated emissivities. It can be seen that the MAD increases slightly with frequency, but is of the order 0.01. The standard deviation of the MAD is 0.006. This implies that NDVI observations in dry conditions can be used to calculate

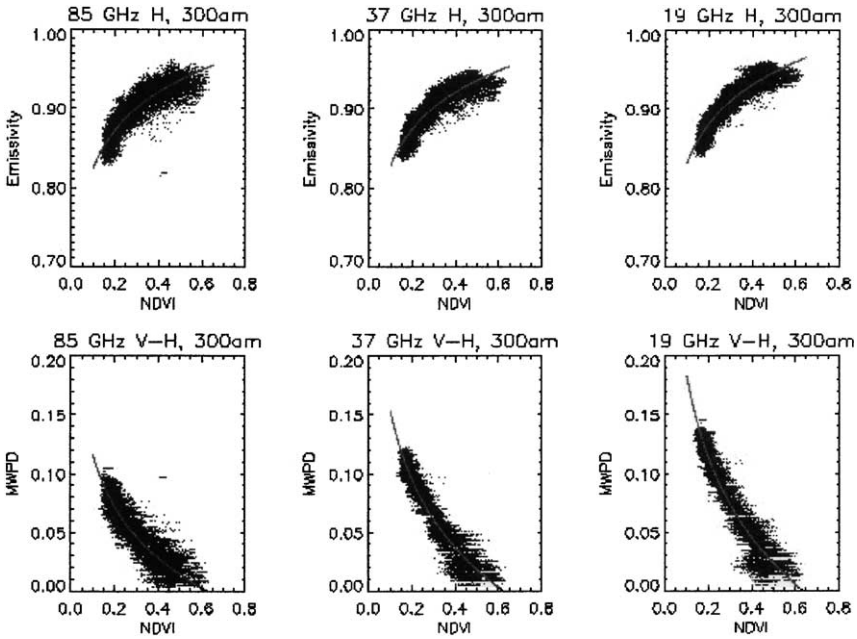

Fig. 5. The H polarisation emissivity and V-H polarisation difference at 19, 37 and 85 GHz plotted against NDVI for dry conditions on 26/10/92. Each point represents a pixel least squares best fit curves are shown as solid lines.

Table 5
The mean coefficients of the fit to H polarisation emissivity and polarisation difference for eight images obtained in dry conditions

Dataset	*a* coefficient (S.D.)	*b* coefficient (S.D.)	*c* coefficient (S.D.)	Mean value of r^2	Mean absolute difference between measured and calculated emissivity (26 October 1992)
85 GHz H	0.996 (0.013)	0.077 (0.009)	0.997 (0.013)	0.78	0.010
37 GHz H	0.988 (0.016)	0.072 (0.010)	0.993 (0.017)	0.83	0.009
19 GHz H	1.001 (0.012)	0.077 (0.008)	1.003 (0.012)	0.86	0.008
85 GHz V–H	−0.099 (0.007)	−0.062 (0.004)	0.334 (0.025)	0.82	0.009
37 GHz V–H	−0.126 (0.011)	−0.082 (0.004)	0.355 (0.033)	0.92	0.008
19 GHz V–H	−0.146 (0.013)	−0.096 (0.005)	0.346 (0.041)	0.92	0.009

The last column gives the mean absolute error in calculating emissivity on 26th October 1992 from NDVI using the coefficients of the mean dry curve.

individual pixel emissivities to within ±0.02 (MAD+2 S.D.) for all frequencies.

6.2. Wet conditions

The microwave emissivity calculated for wet conditions was compared with the appropriate 10-day NDVI composite. Fig. 6 shows the 19-, 37-, and 85-GHz e_H and $(e_V - e_H)$ plotted against NDVI for the morning pass on 31st August 1992. There was heavy rainfall on the 30th August 1992. The average value of the kriged rainfall estimates for 30th August 1992 was 23 mm. Since rainfall in this region generally occurs in the evening or at night, the surface moisture at the time of the early morning pass on 31st August 1992 would probably not have had a chance to evaporate.

The relationship is less clear than under dry conditions with a much greater range of emissivity values for a given NDVI. However, one can still observe a systematic increase in e_H with increasing NDVI and a systematic decrease in $(e_V - e_H)$. In general, e_H values are lower at lower frequencies and the polarisation difference is greater. This is in line with the effect of moisture on e_H being greater at lower frequencies.

The scatter is greater for lower NDVI at all frequencies. This is consistent with the fact that moisture causes a much greater reduction in the emissivity of soil than in the emissivity of vegetation. Spatial variation in soil moisture is reflected in the high variance of e_H at low NDVI where vegetation is sparse and soil emissions form a major part of the observed signal. At high NDVI, the vegetation masks the soil to a much greater extent and the emissivity variance is reduced although it is still high in comparison with the 'dry' data in Fig. 5. This is presumably because of the decreased accuracy of the moist atmospheric correction already mentioned in the sea surface emissivity comparison. These observations agree with those reported

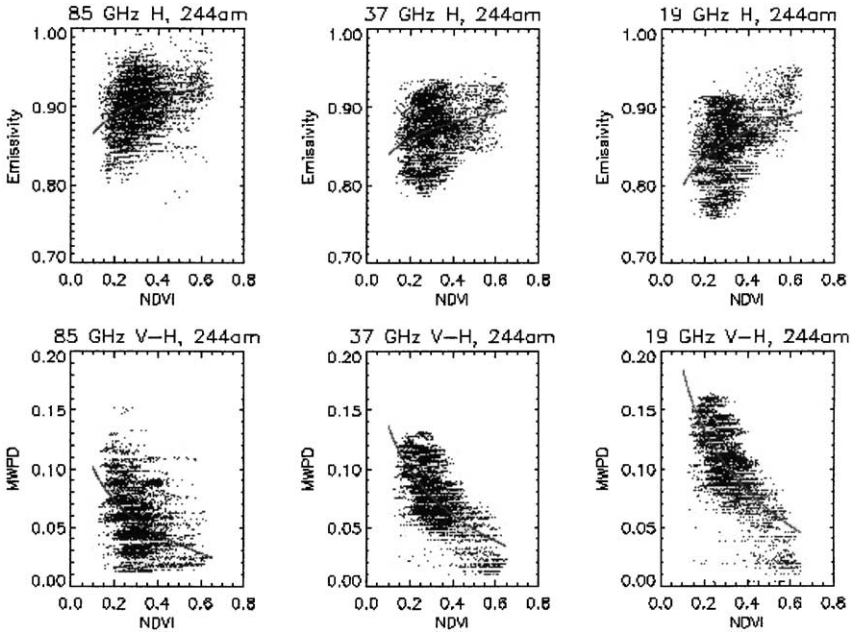

Fig. 6. The H polarisation emissivity and V-H polarisation difference at 19, 37 and 85 GHz plotted against NDVI for wet conditions on 30/08/92. Each point represents a pixel least squares best fit curves are shown as solid lines.

by Morland et al. (2000) for aircraft observations in wet and dry conditions and illustrate the importance of reliable soil moisture data if microwave emissivity is to be estimated after or during rainfall.

6.3. Wet and dry conditions compared

Eight images corresponding to wet conditions were identified in order to compare them with the eight images for dry conditions described earlier. The TIR images coincident with the SSM/I passes were examined to find examples where there was cloud with tops cold enough to indicate rain in the west and clear areas to the east. Since storms normally move from East to West, this situation means that rain has recently fallen over some of the land surface visible in the East. Eight images in August and September (four mornings and four afternoons) were identified, which fulfilled these criteria.

A clearer picture of the relationship between emissivity and NDVI emerges if mean values over selected NDVI ranges are considered. The H emissivities for wet and dry images were binned by NDVI range (0.1–0.2, 0.2–0.3, 0.3–0.4, 0.4–0.5, 0.5–0.7). The lowest range represents bare soil and the highest indicates dense vegetation. The mean e_H in each NDVI bin was calculated for all eight wet passes taken together and all eight dry passes and the results are shown in Fig. 7. The 85-GHz H emissivity is plotted against the centre of the NDVI range, while the 19- and 37-GHz H emissivities are plotted slightly off-centre for clarity. The area covered by each NDVI class is typically several thousand square kilometers. The error bars represent the standard deviation of the pixel emissivity in that NDVI class.

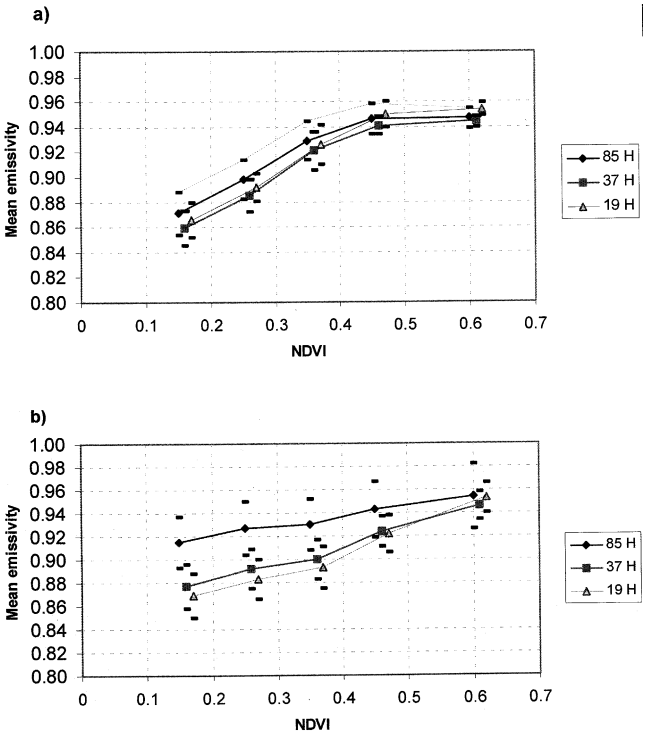

Fig. 7. (a) Mean H polarisation emissivity binned by NDVI range and averaged over eight dry days. 85 GHz emissivity is plotted against the centre of the NDVI range. 19 GHz and 37 GHz are plotted off-centre for clarity. The error bars show the standard deviation of the emissivity in each range. (b) As for (a) but showing results from the eight wet days.

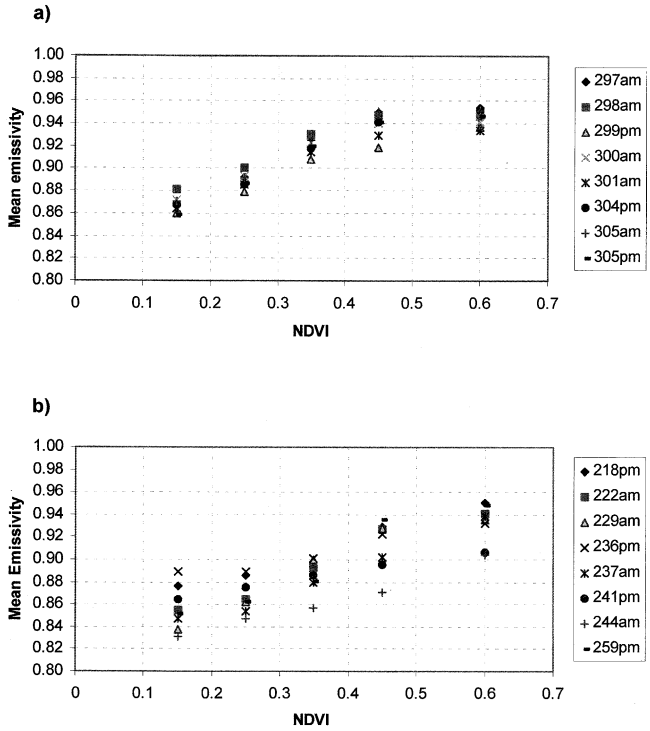

Fig. 8. (a) The mean H polarisation emissivity binned by NDVI range for each of the eight dry days at 19 GHz. (b) As for (a) but showing the eight wet days.

From previously stated arguments, one would expect a reduction in emissivity under wet conditions, which is less at higher frequencies and higher NDVI values. In fact, the observed pattern is more complicated. The mean e_H at 85 GHz is higher for wet data than for dry data, but the standard deviation is also higher. The reason for this is probably that 85 GHz is the channel most subject to errors in the atmospheric correction when the atmosphere is moist and this may be increasing the mean emissivity in wet conditions.

For 19 and 37 GHz, the similarity of the wet and dry mean emissivities at high NDVI conforms to expectation as the vegetation will mask the effect of increased soil moisture. Also for intermediate NDVI values (0.3–0.5), there is the expected decrease in emissivity from dry to wet conditions. However, at low NDVI (0.1–0.3), the emissivities for wet conditions are slightly higher. Plotting the emissivities for the individual days (Fig. 8) throws some light on this. It can be seen that the highest emissivities at low NDVI correspond to afternoon (p.m.) overpasses when the ground surface may have already dried out. The mean value of the morning (a.m.) wet overpasses is in fact lower than the mean dry value.

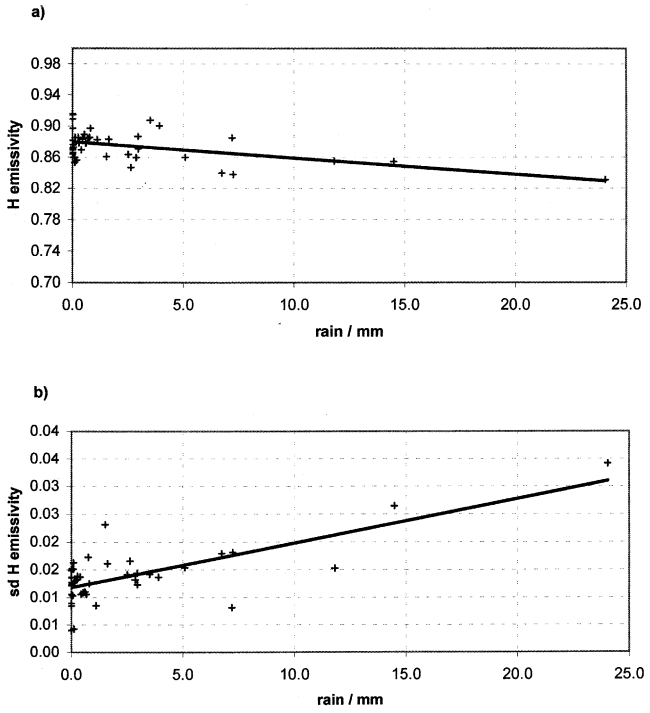

Fig. 9. (a) Mean 19 GHz H emissivity for bare soil plotted against the previous days rainfall for October 1992, (morning passes only). (b) As for (a) but showing standard deviation of emissivity plotted against previous day's rainfall. The least squares best fit line is shown in each case.

Fig. 8 also shows emissivity versus NDVI for individual dry days. It can be seen that the mean emissivity of each dry image increases with NDVI in a consistent manner with a range of ±0.015 at 19 GHz. The mean emissivity of each wet image also increases with NDVI, but there is greater variation between the individual images (up to ±0.03 at 19 GHz) even when morning and afternoon images are considered separately.

These results confirm the consistency of the relationship between NDVI and emissivity under dry conditions. Under wet conditions, there is still a clear relationship between emissivity and NDVI on any individual day, but the variation between days is significantly greater. This is to be expected from the combined effect of spatial and temporal variability in rainfall (and hence soil moisture) and greater error in atmospheric correction. Section 7 discusses whether information on soil moisture can be used to improve the accuracy of the computed emissivities.

7. Relationship between emissivity and soil moisture

7.1. PDR estimates

In an attempt to establish a more quantitative relationship between soil moisture and emissivity, for each morning pass for which data were available, pixels were binned according to the NDVI classes used in Figs. 7 and 8. The mean and standard deviation of e_H were calculated for each NDVI class in each image and compared with the mean PDR for the same set of pixels. The results at 19 GHz for bare soil ($0.1 \leq \mathrm{NDVI} \leq 0.2$) are plotted in Fig. 9. Although there is a high degree of scatter, the emissivity shows the expected decrease with increasing wetness. In contrast, the standard deviation of the emissivity increases with increasing wetness. This is presumably due to both the increase in spatial variability of rainfall with increasing amount, as well as the effect of local variations in soil characteristics and topography. The relationship between PDR and e_V is significantly weaker and is not recorded here.

Table 6 summarises the gradient m, intercept c, and correlation coefficient r^2 for the best linear fit between the mean and standard deviation of e_H and the PDR for all NDVI ranges. In general, the correlation decreases with increasing frequency. The low values of r^2 shown in Table 6 and

Table 6
Parameters for the best linear fit between mean and S.D. of e_H and PDR (morning passes only) for all NDVI ranges and frequencies

			Mean emissivity			S.D. of emissivity		
Frequency (GHz)	No. of days	NDVI (mid-range)	c	m (mm^{-1})	r^2	c	m (mm^{-1})	r^2
19	49	0.150	0.881	−0.0022	0.265	0.012	0.0008	0.542
	49	0.250	0.896	−0.0026	0.286	0.015	0.0010	0.499
	49	0.350	0.919	−0.0027	0.218	0.014	0.0009	0.403
	48	0.450	0.935	−0.0021	0.174	0.014	0.0005	0.147
	39	0.600	0.947	−0.0014	0.100	0.011	0.0005	0.177
37	49	0.150	0.881	−0.0014	0.147	0.013	0.0005	0.293
	49	0.250	0.894	−0.0015	0.174	0.015	0.0007	0.463
	49	0.350	0.916	−0.0022	0.211	0.013	0.0007	0.386
	48	0.450	0.927	−0.0018	0.169	0.013	0.0003	0.100
	39	0.600	0.934	−0.0012	0.098	0.011	0.0005	0.188
85	49	0.150	0.894	−0.0003	0.005	0.020	0.0004	0.093
	49	0.250	0.908	−0.0004	0.008	0.021	0.0004	0.095
	49	0.350	0.930	−0.0007	0.026	0.019	0.0004	0.118
	48	0.450	0.939	−0.0006	0.027	0.019	0.0002	0.032
	39	0.600	0.941	0.0000	0.000	0.018	0.0004	0.048

m is slope, c is intercept, r^2 is correlation coefficient.

exemplified by the scatter in Fig. 9a indicate that a relationship between emissivity and PDR exists but is rather weak. Nevertheless, some consistent patterns emerge. The intercept c (corresponding to dry soil) increases with increasing NDVI and the values agree with the 'dry' results from the smaller data set of Fig. 8a. The slope m is lower for high NDVI, indicative of the reduced effect of moisture on the emissivity of dense vegetation. The masking effect of the vegetation is also apparent in the decrease of r^2 with increasing NDVI. As the soil contributes less to the pixel emissivity, the effect of soil moisture is less significant and the relationship with rainfall is therefore weaker. Interestingly, the PDR is correlated much more strongly with the standard deviation of emissivity than with the emissivity itself. This suggests the intriguing possibility of using the spatial variability of emissivity in a given NDVI class as a means of monitoring rainfall. If this were to be done, the 1-km resolution of the NDVI data means that a reasonable estimate of the emissivity standard deviation for at least some NDVI classes could probably be made at a 1° resolution. The correlation between emissivity standard deviation and rainfall amount also decreases at high NDVI due to vegetation masking.

Of interest is how accurately the areal mean emissivity can be estimated from PDR for a given NDVI range. For zero PDR (dry soil), the calculated standard error on e_H is about ± 0.003 for all NDVI ranges, while for a PDR of 25 mm (wet soil), the standard error is about ± 0.015. While these figures should be treated with some caution because of the small amount of data for high rainfall amounts, they demonstrate that there is some skill in using a combination of vegetation index and PDR to estimate microwave emissivity averaged over several thousand square kilometers. Given that the results are based on a rather simplistic assumption about the relation between soil moisture and rainfall calculated from a sparse rain gauge network, it is likely that much more accurate emissivity values are achievable with better soil moisture data.

Table 7

(a) Parameters for the best linear fit between mean of e_H and soil moisture θ (morning passes only) for all frequencies. m is slope, c is intercept, r^2 is correlation coefficient.

Frequency (GHz)	No. of days	c	m ($\%^{-1}$)	r^2
Morning passes only				
19 H	19	0.95	−0.0100	0.57
37 H	19	0.94	−0.0076	0.56
85 H	19	0.93	−0.0040	0.17
19 (V−H)	19	0.055	0.0049	0.60
37 (V−H)	19	0.044	0.0036	0.59
85 (V−H)	19	0.028	0.0028	0.34

(b) As for (a) but afternoon passes.

Afternoon passes only				
19 H	25	0.92	−0.0037	0.55
37 H	25	0.91	−0.0024	0.35
85 H	25	0.92	−0.0042	0.06
19 (V−H)	25	0.059	0.0021	0.38
37 (V−H)	25	0.051	0.0009	0.15
85 (V−H)	25	0.036	0.0005	0.04

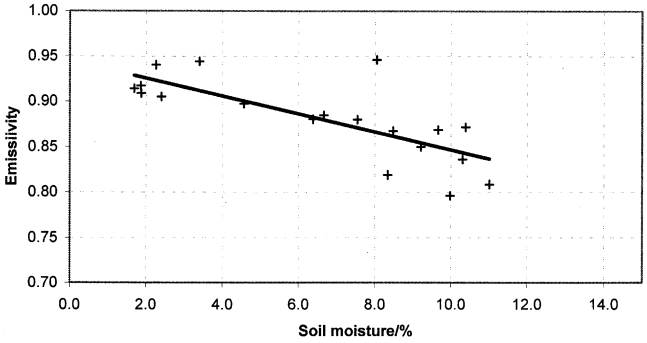

Fig. 10. Mean 19 GHz emissivity for the square 2.2° to 2.7° E and 13.1° to 13.60° N plotted against mean soil moisture from 0 to 5 cm. Solid line is least squares best fit to points.

The same analysis was carried out using polarisation difference ($e_V - e_H$) instead of e_H. The correlations were consistently lower at all frequencies.

7.2. Soil moisture measurements

For each day for which soil moisture measurements were available in the 0–5-cm range, a mean value was calculated and compared with the microwave emissivity averaged over the 0.5° square from 13.1° to 13.6°N and 2.2° to 2.7°E shown in Fig. 4. The size of this square is a compromise between an area small enough to be directly comparable with the point moisture measurements and large enough to contain a significant cloud-free area on most days ('a significant cloud-free area' in this context means >40 cloud-free pixels according to the index defined previously). The range of NDVI in this square is roughly 0.2–0.5 — spanning three of the ranges used in the PDR measurements.

As for the PDR data, a best fit linear relationship between the percentage soil moisture θ and e_H or polarisation difference ($e_V - e_H$) was determined. The results are summarised in Table 7 and are in qualitative agreement with the PDR data reported above. As expected, emissivity decreases with increasing θ and the rate of decrease (indicated by the slope m of the linear relationship in Table 7) is lower at higher frequencies. e_H is more sensitive than e_V to moisture changes (larger m) and has a higher correlation at all frequencies. The correlation is also higher at all frequencies for the morning overpasses, reflecting the fact that most moisture measurements were made in the morning. In contrast to the PDR results, polarisation difference shows a slightly stronger relationship (greater r^2) than the emissivity itself.

Although the r^2 values appear to indicate a much better correlation for emissivity with soil moisture observations than with PDR, this is mainly a result of the difference of numbers of data points in the regression. A Student's t test shows in fact that both regressions have a similar significance ($P \leq 0.0003$). The standard error for emissivity values calculated from the regression line is ~ 0.015.

Fig. 10 shows the 19-GHz H emissivity plotted against soil moisture. The decrease in emissivity between the

extremes of dry (θ = 0%) and wet (θ = 12%) is roughly comparable with the change observed for PDR between 0 and 25 mm for NDVI in the range 0.2–0.4.

Both the PDR and the soil moisture results are in qualitative agreement with previously reported results from ground and aircraft measurements (e.g., Morland et al., 2000) showing that soil moisture generally decreases emissivity, increases polarisation difference, and increases the range of observed emissivity.

8. Conclusions

A method has been demonstrated for the calculation of microwave emissivity from SSM/I observations, Meteosat TIR data, and the ECMWF analysis of atmospheric temperature and water vapour. The emissivity of the sea surface calculated using this method agreed with theory to within ±0.034 in an area with a dry atmospheric profile. In an area with a moist atmospheric profile, the agreement was poorer, being to within ±0.072 or less apart from the 85-GHz H channel where the discrepancy was as much as 0.174. The fact that the measured sea surface emissivity was consistently greater than the calculated emissivity for the moist profile suggests that the atmospheric correction is underestimated. As land surface emissivities are considerably higher than that of water, the figures quoted here represent a conservative upper bound on the errors expected for land surface emissivities.

This study shows that there is a clear, nonlinear relationship between microwave emissivity and NDVI when the surface is dry. The pixel H emissivity and polarisation difference can be predicted to an accuracy of ±0.02 in dry conditions if the NDVI is available. This is a useful result since it can establish the microwave emissivity at the beginning of a rainfall period.

In wet conditions, the lowest e_H values generally occur for the lowest NDVI values. However, there is a much greater spread of emissivity for a given NDVI. This is attributable to variations in rainfall and surface characteristics across each 5° square image, as well as the higher errors in the emissivity calculation when the atmosphere is moist.

In order to quantify the effects of surface wetness on emissivity, the PDR and ground-based soil moisture measurements were used as indicators. In both cases, results were best for 19-GHz H polarisation and polarisation difference. At this frequency, a combination of NDVI and PDR can estimate mean e_H over an area of several thousand square kilometers with a standard error of ±0.003 in dry conditions or ±0.015 after 25 mm of rainfall. The error on estimates based on soil moisture measurements within a limited vegetation range was comparable. The lower correlations obtained for afternoon overpasses demonstrate the rapidity with which soil dries out in a semiarid environment and emphasize the need for contemporaneous soil moisture and emissivity in any such future studies. These results were based on a very limited amount the data and more work needs to be done in this area, however, there is a strong suggestion that useful estimates of microwave emissivities for frequencies < 40 GHz can be made from a combination of vegetation and moisture indicators.

The results show that wetted areas can be mapped by observing microwave emissivity changes between wet and dry conditions. They also show that spatial variability in emissivity can be linked to the PDR. In terms of accurate retrievals of rainfall from PMW sensing over land surfaces, however, there is still some way to go. It is clear that improvement is needed both in quantifying soil moisture and in understanding its effect on surface emissivity particularly in partly vegetated areas. For more accurate modeling of soil moisture, more accurate data on rainfall, potential evaporation, and soil characteristics are needed. For much of Africa, ground-based data of this kind are not a realistic aspiration. Alternatively, one can hope for better measurements of soil moisture from space-borne sensors. At present, there is no method of directly measuring soil moisture from space but in the longer term there will be sensors operating at lower microwave frequencies (1.4 and 6 GHz), which can measure soil moisture in the top 6 cm of the soil. These will have a spatial resolution of 30–60 km, which is comparable to the resolution of the SSM/I sensor. A comparison of the soil moisture estimated from these sensors with microwave emissivity estimates would contribute greatly to our understanding of how emissivity is affected by soil moisture on the satellite scale and provide a means of filtering out the land surface contribution from remotely sensed microwave radiances leading improved rainfall estimates over land.

Acknowledgments

The authors gratefully acknowledge the help of Rogerio Bonifacio with the data analysis and interpretation. We would also like to thank the following people and organisations for making data and models available: ECMWF — SSM/I data, atmospheric water, and temperature profile; TAMSAT group (University of Reading) — TIR data; S.J. English (UK Met Office) — microwave atmospheric correction model; K.P. Shine (University of Reading) — infrared atmospheric correction model; G. Dugdale (University of Reading) — meteorological data; Agrhymet — CILSS daily rainfall data; LTHE group from ORSTOM (now IRD) — EPSAT daily rainfall data; Hapex Sahel Information System for the following; Y. Kerr — AVHRR data; B. Monteny — meteorological data and rainfall data; A. Chanzy, J.D. Cooper, H. Stricker — soil moisture data.

References

Basist, A., Grody, C., Peterson, T. C., & Williams, C. N. (1998). Using the special sensor microwave/imager to monitor land surface temperatures, wetness and snow cover. *Journal of Applied Meteorology*, *37*, 889–911.

Calvet, J. C., Wigneron, J. P., Chanzy, A., & Haboudane, D. (1995). Retrieval of surface parameters from microwave radiometry over open canopies at high frequencies. *Remote Sensing of Environment*, *53*, 46–60.

Chanzy, A. (1995). Data from Hapex Sahel experiment on CD-ROM produced by Hapex Sahel information. LERTS, Toulouse, France.

Choudhury, B. J. (1993). Reflectivities of selected land surface types at 19 and 37 GHz from SSM/I observations. *Remote Sensing of Environment*, *46*, 1–17.

Choudhury, B. J., & Blanchard, B. J. (1983). Simulating soil water recession coefficients for agricultural watersheds. *Water Resources Bulletin, American Water Resources Association*, *19* (2), 241–247.

Choudhury, B. J., Schmugge, T. J., Chang, A., & Newton, R. (1979). Effect of surface roughness on the microwave emission from soils. *Journal of Geophysical Research*, *84* (C9), 5699–6706.

Cooper, J. D. (1995). Data from Hapex Sahel experiment on CD-ROM produced by Hapex Sahel information. LERTS, Toulouse, France.

Dugdale, G. (1995). Data from Hapex Sahel experiment on CD-ROM produced by Hapex Sahel information. LERTS, Toulouse, France.

English, S. J. (1995). Airborne radiometric observations of cloud liquid water emission at 89 and 157 GHz: application to retrieval of liquid water path. *Quarterly Journal of the Royal Meteorological Society*, *121*, 1501–1524.

English, S. J. (1999). Estimation of temperature and humidity profile information from microwave radiances at different surface types. *Journal of Applied Meteorology*, *38* (10), 1526–1541.

English, S. J., & Hewison, T. J. (1998). A fast generic millimeter wavelength emissivity model. *Proceedings of SPIE*, *3503*, 288–299.

European Centre for Medium Range Weather Forecasting (1995). MARS — Meteorological Archive and Retrieval System M1.9/2, ECMWF Computer Bulletin B 6.7/2.

Hallikainen, M. T., Ulaby, F. T., Dobson, M. C., El-Rayes, M. A., & Wu, L. K. (1985). Microwave dielectric behavior of wet soil: Part I. Empirical models and experimental observations. *IEEE Transactions on Geoscience and Remote Sensing*, *GE-23* (1), 25–34.

Herman, A., Kumar, V. B., Arkin, P. A., & Kousky, J. V. (1997). Objectively determined 10-day African rainfall estimates created for famine early warning. *International Journal of Remote Sensing*, *18* (10), 2147–2160.

Jackson, T. J. (1997). Soil moisture estimation using Special Satellite Microwave Imager satellite data over a grassland region. *Water Resources Research*, *30* (6), 1475–1484.

Jackson, T. J., Kostov, K. G., & Saatchi, S. S. (1992). Rock fraction effects on the interpretation of microwave emission from soils. *IEEE Transactions on Geoscience and Remote Sensing*, *GE-30* (3), 610–616.

Jackson, T. J., & O'Neill, P. E. (1988). Observed effects of soil organic matter content on the microwave emissivity of soils. In: IGARSS '88, Edinburgh, Scotland, 13–16th Sept. (pp. 673–676) (ESA SP-284).

Jones, A. S., & Vonder Haar, T. H. (1997). Retrieval of microwave surface remittance over land using coincident microwave and TIR satellite measurements. *Journal of Geophysical Research*, *102* (D12), 13609–13626.

Journel, A., & Huijbregts, C. H. (1978). *Mining geostatistics*. New York: Academic Press (600 pages).

Kerr, Y. H., Lagouarde, J. P., & Imbernon, J. (1992). Accurate land surface temperature retrieval from AVHRR data with use of an improved split window algorithm. *Remote Sensing of Environment*, *41*, 197–209.

Kummerow, C., & Giglio, L. (1994). A passive microwave technique for estimating rainfall and vertical structure information from space: Part II. Applications to SSM/I data. *Journal of Applied Meteorology*, *33*, 18–34.

Lebel, T., Sauvageot, H., Hoepffner, M., Desbois, M., Guillot, B., & Hubert, P. (1992). Rainfall estimation in the Sahel: the EPSAT Niger experiment. *Hydrological Sciences Journal*, *37* (3), 201.

Matthews, E. (1983). Global vegetation and land use: new high resolution data base for climate studies. *Journal of Climate and Applied Meteorology*, *22*, 474–486.

Mätzler, C. (1994). Passive microwave signatures of landscapes in winter. *Meteorological and Atmospheric Physics*, *54*, 254–260.

Meteosat Exploitation Project (1989). Meteosat-4 Calibration Report, Issues 1–21. European Space Operations Centre, Darmstadt, Germany.

Monteny, B. (1995). Data from Hapex Sahel experiment on CD-ROM produced by Hapex Sahel information. LERTS, Toulouse, France.

Morland, J. C., Grimes, D. I. F., Dugdale, G., & Hewison, T. J. (2000). The estimation of land surface emissivities at 24 GHz to 157 GHz using remotely sensed aircraft data. *Remote Sensing of Environment*, *73*, 323–336.

Prigent, C., Rossow, W. B., & Matthews, E. (1997). Microwave land surface emissivities estimated from SSM/I observations. *Journal of Geophysical Research: Atmospheres*, *102* (D18), 21867–21890.

Shine, K. P. (1991). On the cause of the relative greenhouse strength of gases such as the halocarbons. *Journal of Atmospheric Science*, *48*, 1513–1518.

Sreenivas, K., Venkataratnam, L., & Narasimha Rao, P. V. (1995). Dielectric properties of salt-affected soils. *International Journal of Remote Sensing*, *16* (4), 641–649.

Stricker, H. (1995). Data from Hapex Sahel experiment on CD-ROM produced by Hapex Sahel information. LERTS, Toulouse, France.

Thorne, V., Coakeley, P., Grimes, D. I. F., & Dugdale, G. (2001). Comparison of TAMSAT and CPC rainfall estimates for southern Africa, accepted for publication. *International Journal of Remote Sensing*,.

Ulaby, F. T., Moore, R. K., & Fung, A. K. (1981). *Microwave remote sensing: active and passive: Vol. I. Microwave remote sensing fundamentals and radiometry*. Norwood, MA: Artech House.

Valor, E., & Caselles, V. (1996). Mapping land surface emissivity from NDVI: application to European, African and South American areas. *Remote Sensing of Environment*, *57*, 167–184.

Van de Griend, A. A., & Owe, M. (1993). Determination of microwave vegetation optical depth and single scattering albedo from large scale moisture and Nimbus/SMMR satellite observations. *International Journal of Remote Sensing*, *14* (10), 1875–1886.

Wigneron, J.-P., Kerr, Y. H., Chanzy, A., & Jin, Q. J. (1993). Inversion of surface parameters from passive microwave measurements over a soybean field. *Remote Sensing of Environment*, *46*, 61–72.

Xiang, X., & Smith, E. A. (1997). Feasibility of simultaneous surface temperature–emissivity retrieval using SSM/I measurements from Hapex Sahel. *Journal of Hydrology*, *188–189*, 330–360.